^{19}F MRI Tracking of Inflammation for Earlier Prediction of Colitis-Associated Cancer

by
Soo Hyun Shin

A thesis submitted to Johns Hopkins University in conformity with the requirements for the degree of Master of Science in Engineering

Baltimore, Maryland
April, 2014

Abstract

Colitis-associated cancer (CAC) develops through complication of inflammatory bowel diseases (IBD) such as ulcerative colitis (UC) and Crohn's disease (CD). Currently, CACs can only be diagnosed by colonoscopy and biopsy, which are invasive and prone to sampling errors. In this study, the feasibility of using ^{19}F MRI for earlier diagnosis of CAC development was investigated by serial imaging of inflammatory sites in the colon. *In vivo* MR imaging of CAC-induced mice showed patchy distributions of ^{19}F signals on colon wall, and co-localization of ^{19}F signal patches with dysplastic and inflammatory lesions were confirmed by *ex vivo* imaging. Histological scores of inflammation and dysplasia showed significant correlation with the intensity of ^{19}F signals. Overall, ^{19}F MRI was used for the first time to observe the early stage of carcinomatous change of inflammatory sites in the colon, which is expected to enable earlier diagnosis of CAC. Thewell established relationship between inflammation and cancer suggests that ^{19}F MRI can also be used in early diagnosis of wide range of cancer types.

Acknowledgements

First of all, I should thank Dr. Jeff Bulte for offering me a chance to study the exciting field of cellular imaging and for all the advice and guidance he provided throughout my Master's study. I am also grateful to Dr. PiotrWalczak and Dr. MiroslawJanowski for all the advice and comments on this thesis writing. Special thanks should be given to Deepak Kadayakkara, who suggested this study to me as my thesis work and helped throughout the whole experiments and manuscript writing, even after leaving to Springfield. I also acknowledge Dr. Cory Brayton for her expert opinion on histology as a pathologist, which was indispensable for completing this work. Irina Shats has devoted to this study by preparing tissue sections and providing other technical assistance, which I truly appreciate. I would like to thank Lea Fortuno-Miranda, who has arranged and prepared numerous reagents that were used in this work. I should also thank other lab members, Dian Arifin, Mangesh Kulkarni, Antje Arnold, Anna Jablonska, Amit Srivastava, MoussaChehade, Laura Rose, Sujith Sajja and Michael Korrer who have never hesitated to help me when needed throughout my study.

Lastly, but not least, my special and profound thanks go to my family, who have always been supporting me from Korea—my parents, Seung Joon Shin and Young Joo Byun, my brother and his wife, Woo Hyun Shin and Charang Hahm, and my lovely newborn niece, Hajeong Shin.

Table of Contents

List of Figures

1. Introduction

1.1 Inflammatory Bowel Diseases (IBD) and Colitis-Associated Cancer (CAC)

The causal relationship between inflammation and cancer has been well established (Fig. 1) (1). Epidemiological studies of patients and genetically modified mice have shown that chronic inflammation increases the risk of developing many types of cancer including bladder, cervical, gastric intestinal and thyroid cancer(2, 3). In molecular perspective, the transcription factors such as NF-κB, STAT3, and HIF1α in tumor cells recruit the inflammatory cells, which then promote angiogenesis, tumor cell proliferation, survival, migration, and metastasis (2, 4, 5). While it is estimated that the underlying inflammation is linked to 15 - 20% of cancer mortality worldwide, appropriate treatment with anti-inflammatory agents has shown to decrease the incidence and mortality of several types of tumor (6, 7, 8).

The most representative relationship between inflammation and cancer is seen in colon through inflammatory bowel diseases (IBD) followed by the development of colitis-associated cancer (CAC). IBD such as ulcerative colitis (UC) and Crohn's disease (CD) are prevalent chronic inflammatory disorders of intestine in the United States with 1 - 1.5 million patients affected (9, 10). The chronic inflammation accompanied by IBD is characterized by infiltrated immune cells producing proinflammatory cytokines and reactive oxygen species which facilitate mutations in oncogenes and tumor suppressor genes such as p53, adenomatous polyposis coli (APC), and K-ras (11). Sustained inflammation accumulates these mutations in colonic epithelial cells and leads to the development of colorectal cancer (CRC), which in this case is called CAC.

CACs show several characteristics different from sporadic CRCs in developing stages (12). In molecular level, CRCs and CACs share similar molecular alterations, but the timing and frequency of these alterations are major difference. In CRC, loss of APC function occurs in early stage of the pathogenesis and leads to the progression of adenoma. The alteration of p53 gene function then follows to drive the carcinomatous change of the adenomas. In CAC, p53 plays more important role in the early event while the alteration of APC function is much less frequent than in CRC and occurs in the late stage of pathogenesis. In a macroscopic view, CRCs develop through the sequence of adenoma-carcinoma, in which adenomas are usually polypoid and focal. CACs, however, develop through the sequence of inflammation-dysplasia-carcinoma, and the dysplastic lesions are usually multifocal and flat (13), which makes the detection of lesions much more difficult and hinders the early diagnosis and treatment.

Previously, it was shown that the risk of CAC is directly correlated with the duration of IBD and severity of inflammation (14). Meta-analysis showed that the risk of developing CAC is 2% after 10 years of UC, 8% after 20 years, and 18% after 30 years (15, 16). In case of CD, the risk for CAC is 2.9% at 10 years of disease, which increases to 8.3% after 30 years (17, 18). Thus, IBD patients are recommended to take regular surveillance every 1 - 2 years after 8 - 10 years from the onset of disease. The high incidence rate in young ages between 16 and 30 years (19) and the increased risk for carcinogenesis further elevate the patients' burden.

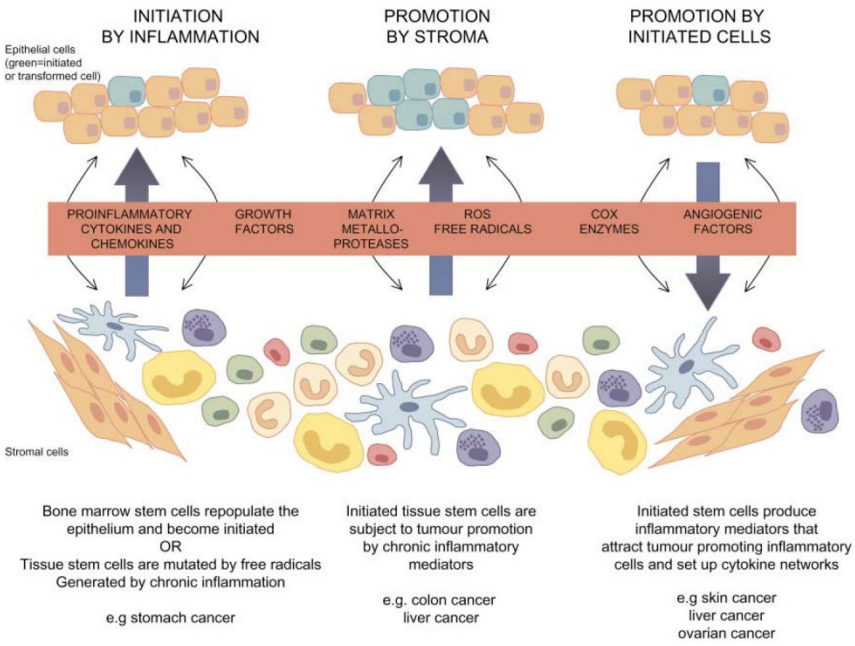

Figure 1. Mechanisms of inflammation-driven cancer development (Ref. 3). Epithelial cells and tissue stem cells are genetically altered by proinflammatory cytokines or free radicals, and chronic inflammatory mediators facilitate tumor promotion. The tumor-initiated epithelial cells in turn produce inflammatory mediators which recruit more inflammatory cells for further tumor promotion.

1.2 Current Diagnosis: Endoscopy and Biopsy

Most of the current diagnoses of IBD and colon cancer are based on endoscopy and mucosal biopsy (20, 21). For the diagnosis of IBD, endoscopy aids in distinguishing UC from CD and defining the patterns and extent of mucosal inflammation. Once the IBD is diagnosed, endoscopy accompanied by histological analysis of biopsies are used to observe the severity of inflammation involvement and make therapeutic decisions. Especially in long-term complication of IBD, endoscopy is indispensable for monitoring any development of dysplastic lesions which can further develop into invasive carcinoma.

Yet, current endoscopy has a limitation of low magnification which only allows the surveillance of mucosal surface and surrounding blood vessels (22). Microscopic abnormalities cannot be observed, and this limitation becomes a huge drawback in the diagnosis of colitis-associated neoplasms. Due to the similar morphology, differential diagnosis between raised colitis-associated neoplasm and sporadic colorectal adenoma based on macroscopic appearance is difficult (23, 24), while the former should be treated by colectomy and the latter by polypectomy (25). Since colitis-associated neoplasms are usually in flat mucosa, it was reported that 50% - 80% of dysplastic lesions rising from colitis are not visible by endoscopy (26). Thus mucosal biopsies must be taken and analyzed to detect any flat colitis-associated dysplastic lesions. Although specific guidelines for biopsy were suggested, such as performing at least 32 biopsies per surveillance and obtaining samples every 10 cm (27), still it is not free from sampling errors.

New endoscopic imaging techniques are being studied to overcome the limitations. Chromoendoscopy reveals more detailed mucosal surface by spraying various dyes on

mucosal surface (28), and narrow band imaging improves blood vessel imaging by adopting optical filters which narrow the bandwidth of spectral transmittance (29). Confocal laser endomicroscopy was recently introduced for *in vivo* imaging of mucosal layer with 1,000-fold magnification, capturing cellular and subcellular features of lesions (30).

Although these new technologies have shown much improvement in detection of colitis-associated neoplasia, they are high cost methods and still invasive imaging modalities which cause patient discomfort. Considering that the IBD patients should frequently undergo the surveillance for a long time, the cost and invasiveness are major issues to be solved. Thus, non-invasive imaging modality which detects inflammatory and dysplastic lesions and measures their severity is needed.

1.3 Non-invasive Imaging of Inflammation

Chronic inflammation is caused by variety of reasons, including persistent injury and microbial infection, prolonged exposure to a toxic agent, and autoimmune diseases, in which the immune responses damage the host tissue and result in tissue injury and inflammation. A group of immune cells such as lymphocytes, plasma cells and macrophages infiltrate to the inflammatory sites and contribute on tissue destruction and repairing with fibrosis and angiogenesis (31). In case of IBD, the mucosal barrier is breached by infectious or toxic agent, and the immune cells in lamina propria are persistently exposed to the luminal bacteria which initiate and maintain the inflammatory cascade (32). The tissue injury caused by chronic inflammation is histologically

represented by structural abnormalities such as goblet cell depletion, crypt loss, ulceration and erosion (33).

Positron emission tomography (PET) and computer tomography (CT) has been tested to non-invasively image colon and quantify inflammation by targeting high metabolic activity in inflammatory lesions (34). PET involves using 18-fluorodeoxyglucose (^{18}FDG) for measuring abnormal metabolism with high glycolytic rates in several diseases including malignancy, inflammation and infection (35). PET complemented with CT for anatomical context was shown to be effective in diagnosis of IBD with a good correlation between PET activity and severity of inflammation. However, PET involves a radioactive tracers and has high background and low spatial resolution.

Magnetic resonance imaging (MRI) was also evaluated as a possible non-invasive modality for monitoring IBD patients (36, 37). MRI overcomes the limitations of PET/CT, since it does not generate ionizing radiation and has high spatial and temporal resolution with sufficient soft tissue contrast. However, MRI of bowel is difficult due to the complex three dimensional anatomies and inhomogeneity of magnetic field. Previous studies on application of MRI in IBD diagnosis only used colon wall thickness as a parameter of disease activity, which can never be a thorough evaluation.

Recent advancements in nanotechnologies led to the development of novel contrast agents of MRI, such as superparamagnetic iron oxide (SPIO) nanoparticles and perfluorocarbon (PFC) nanoemulsions. Intracellular labeling of these contrast agents enables non-invasive visualization of cells of interest, which has been widely used in biomedical studies including stem cell therapy and cancer diagnosis (38). By specifically

labeling immune cells and tracking them, the possibility of applications in immunotherapy and diagnosis of inflammatory diseases was also demonstrated (39).

1.4 SPIO Nanoparticle

SPIO nanoparticles affect T2 with strong magnetic moment from ferrous and ferric oxide cores (40). This strong local magnetic perturbation affects the surrounding water protons and leads to signal loss on T2-weighted MR images. Thus, the cells labeled with SPIO nanoparticles are expressed as dark spots on MR images due to the negative contrast. Upon systemic injection, SPIO nanoparticles are taken up by cells from reticuloendothelial system (RES), such as blood monocytes and macrophages. This approach has been applied to broad range of inflammatory events, including graft rejection and atherosclerosis (41, 42). The involvement of macrophages in neuroinflammation has further broadened the application of SPIO nanoparticles into neural diseases such as stroke, multiple sclerosis and brain tumors (43 - 45).

Although SPIO nanoparticles turned out to be useful in imaging inflammatory sites, it is difficult to measure and quantify the severity of inflammation due to its non-linear response to external magnetic field. Negative contrast also makes the interpretation of MR images difficult, especially in case of hemorrhage near to lung, bone or blood flow (46). Another challenge is that SPIO particles can remain in a region of interest even after the labeled cells die and generate false signal. These limitations should be overcome for more accurate assessment of inflammation.

1.5 PFCNanoemulsion and ^{19}F MRI

PFC is a molecule with similar structure to common organic molecules except that all the hydrogen atoms are substituted by fluorine. It is one of the most biologically inert molecules ever produced so that no enzyme can metabolize PFC (47, 48). Still, PFC is non-toxic *in vivo* even at high doses due to its high hydrophobicity and lipophobicity (49). Most PFCs have high oxygen solubility, which initiated early biological application of PFCs as blood substitutes for human use (50, 51). Thus the safety issues have been well studied and PFC has high potential of clinical usage.

^{19}F MRI with PFC emulsion as a probe is considered as a strong candidate for non-invasive imaging method for detecting inflammatory sites (39, 52, 53). Unlike ^{1}H MRI with SPIO nanoparticle labeling, PFC emulsions function as tracer agents so that ^{19}F MRI directly detects the ^{19}F nuclei in labeled cells. The absence of endogenous ^{19}F in biological tissues ensures that there is no background and the "hot spots" only represent the labeled cells. Since the ^{19}F signal is directly proportional to the number of ^{19}F atoms, the exact number of labeled cells in a region of interest can be quantified. Thus ^{19}F MRI overcomes the complexity of ^{1}H MRI interpretation and enables quantification of cell numbers, or severity of inflammation (54, 55).

Once PFC emulsions are intravenously injected, a subgroup of leukocytes including monocytes, macrophages, neutrophils, dendritic cells and B lymphocytes are labeled with macrophages internalizing most of the agents (56 - 59). Since macrophages are crucial mediators of chronic inflammation (60, 61), selectively labeling macrophages enables imaging inflammatory loci with "hot spots" of MR signal and measuring the

severity of inflammation in several diseases, such as pulmonary inflammation, multiple sclerosis, ischemia, tumor and IBD (52, 57, 58, 62, 63).

1.6 Study Summary

In this study, ^{19}F MRI was used for the first time to longitudinally image the inflammatory sites in mouse IBD model developing to dysplastic lesions. Azoxymethane (AOM) and dextran sulfate sodium (DSS) were used to induce CAC development in mice (64, 65). *In vivo* ^{19}F MRI showed the inflammatory sites on colon wall and *ex vivo* MRI was done to exactly co-localize the ^{19}F signals with any inflammatory sites and development of CAC. To confirm that ^{19}F signals represent higher severity of inflammation and risk of CAC development, histological grading of inflammation and dysplasia was done and correlated with normalized signal-to-noise ratio (SNR) of ^{19}F images. Overall, this study demonstrates that ^{19}F MRI is an effective non-invasive imaging modality for tracking inflammatory sites and thus for predicting future sites of CAC development. It is expected that this technique can be widely used in diagnosis and treatment of other types of cancers that are driven by inflammation.

2. Methods

2.1 Mouse Model of CAC

All the experimental procedures involving animals were approved by Institutional Animal Care and Use Committee (IACUC) at the Johns Hopkins University.For a mouse model that develops CAC, the protocol previously described was used (64, 65). Briefly, 8-week-old female A/J mice (n = 5) purchased from Jackson Laboratories (Bar Harbor, ME, USA) were intraperitoneally injected with 10mg/kg body weight of AOM (A2853, Sigma, St.Louis, MO, USA) at day 0. To ensure that tumors develop through IBD, DSS (160110, MP Biomedicals, Solon, OH, USA) was used to induce chronic inflammation in a colon. DSS was dissolved in drinking water (2.5% w/v) for mice every 3 weeks until week 7 (Fig. 2). Mice weights were measured every week until the animals were sacrificed.

2.2 PFC Emulsion Administration

Two days before the first *in vivo* MR imaging, mice were injected with 200µl of a commercially available perfluoro-15-crown-5-ether emulsion (VS-580H, Celsense, Pittsburgh, PA, USA) intravenously through a tail vein using $27_{1/2}$G needle. The concentration of the emulsion is 200 mg/ml, and the diameter ranges from 145 to 165 nm according to the manufacturer.

2.3 In vivo MR Imaging

Mice were imaged every 15 days from day 50 to day 110. Imaging was performed using an 11.7 T Bruker Scanner and a surface coil tunable to both ^{1}H and ^{19}F

(BrukerBiospin, Billerica, MA, USA). The mice were anesthetized by 1.5% isoflurane gas and heart rate was monitored during the imaging sessions. ^{1}H images were acquired using a rapid acquisition with refocused echoes (RARE) sequence (Parameters: Slice thickness = 2 mm, Matrix size= 256 x 256, RARE factor = 8, FOV = 3.2cm x 2.0cm, NA = 4, Repetition time (TR)/Echo time (TE) = 1200ms/30ms). ^{19}F images were also acquired by the same sequence (Parameters: Slice thickness = 2 mm, Matrix size = 64 x 32, RARE factor = 8, FOV = 3.2cm x 2.0cm, NA = 64, TR/TE = 1000ms/14ms). ^{19}F images were expressed in pseudo color scale and superimposed to the corresponding ^{1}H images. Each image was scaled for optimal visualization and presentation.

2.4 Ex vivo MR Imaging

After the last *in vivo* MR imaging, the mice were euthanized and the colons were excised. Each colon was divided into two parts, ascending colon and descending colon, and a glass rod was inserted into the lumen of each colon segment to straighten the tissues. After fixation in 4% paraformaldehyde for 2 days, tissues were transferred to PBS and imaged with 750 MHz MR microimaging system and a 25mm-volume coil tunable to either ^{1}H or ^{19}F (BrukerBiospin, Billerica, MA, USA). Again, ^{1}H and ^{19}F images were acquired using a RARE sequence (^{1}H Parameters: Slice thickness = 1 mm, Matrix size = 256 x 256, RARE factor = 8, FOV = 2.60 cm x 1.30 cm for sagittal and 1.30 x 1.30cm for axial images, NA = 4, TR/TE = 1000ms/10ms), and ^{19}F images (Matrix size = 64 x 32, RARE factor = 16, NA = 256, TR/TE = 1000ms/6ms. Other parameters are same as ^{1}H images) were superimposed to the according ^{1}H images.

2.5 ^{19}FMR Signal Analysis

For analysis of ^{19}F MR signal, ParaVision 5.1 software (BrukerBiospin) was used. Region of interest (ROI) was drawn on each^{19}F signal patch on colon wall for measuring mean intensity. The standard deviation of the background intensity was also measured to calculate signal-to-noise ratio (SNR) of the selected ^{19}F signal patch. Each ^{19}F MR image was adjusted so that only the ^{19}F signals with SNR of 3.5 or above remain and background noises are suppressed. SNR of ^{1}H images were also calculated by the same method with the whole mouse body or excised colon considered as a signal. ^{19}F SNRs normalized by corresponding^{1}H SNRs were used throughout the study as an indicator of signal intensity.

2.6 Histological Grading of Inflammation and Dysplasia

Fixed colon tissues were washed with PBS and were cut longitudinally to investigate a possible tumor outgrowth. Colon tissues were further divided into multiple segments and classified into either segments with ^{19}F signals or those without the signals. These segments were embedded in paraffin block and cut transversely into 5μm-thick sections, followed by hematoxylin and eosin (H&E) staining. The sections were analyzed by two pathologists blinded to the identity of samples. The degree of inflammation was scored based on the method proposed by Hogan et al. with some modification (66). Briefly, degree of inflammation was assessed in six categories which are 1) area involved, 2) crypt loss, 3) erosion/ulceration, 4) edema, 5)polymorphonuclear cell (PMNC) infiltration and 6) mononuclear cell (MNC) infiltration. For area involved and crypt loss, the severity was scaled as 0, normal; 1, 0~10%; 2, 10~25%; 3, 25~50%; and 4, 50% or

above. Erosions and ulcerations were defined as 0, intact epithelium; 1, involvement of the lamina propria; 2, ulcerations involving the submucosa; and 3, transmural ulcerations. The rest of the parameters were scored as 0, absent; 1, weak; 2, moderate; 3, severe. Total colitis score was expressed as the sum of all scores from individual parameters. Any appearance of adenomas and dysplastic lesions was also graded based on their sizes and invasiveness: 0, none; 1, <1 mm; 2, 1 ~ 3 mm; 3, >3 mm or clear invasion.

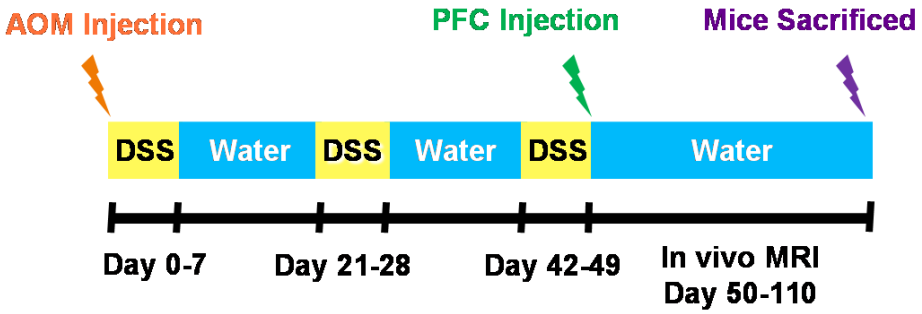

Figure 2. Timeline of developing CAC mouse model. Single intraperitonealinjetion of azoxymethane (AOM) was made on day 0 with the first cycle of DSS started simultaneously. Each DSS cycle was a week-long, applied every three weeks until week 7. On day 48, at the end of the last DSS cycle, PFC emulsions were intravenously injected through a tail vein and *in vivo* MR imaging was performed through day 50 to day 110 until mice were sacrificed.

3. Results

3.1 In vivo MRI Shows Inflammatory Sites on Colon Wall

Chronic inflammation was induced by a single injection of AOM and three cycles of DSS solution treatment (Fig.2). At the end of the last cycle of DSS treatment, PFC emulsion was injected to both CAC-induced and control group of mice. The *in vivo* imaging of mice was initiated 2 days after the PFC injection. ^{19}F MRI showed PFC emulsions concentrated on a colon wall with patchy distribution (Fig. 3A). No ^{19}F signals were detected from colon wall of mice that were not induced with CAC (Fig. 3B). Along with ^{19}F signals, proliferative lesions started to be observed from CAC-induced mice on day 80. To investigate the change of ^{19}F signal intensity over time, SNR of ^{19}F signals on colon wall was normalized to the SNR of corresponding ^{1}H images. The normalized SNR showed that the ^{19}F signal intensity kept decreasing over time, but the signals were detected up to day 110 when the mice were euthanized (Fig. 3C). Strong ^{19}F signals were detected from the vertebra and spleen of all mice.

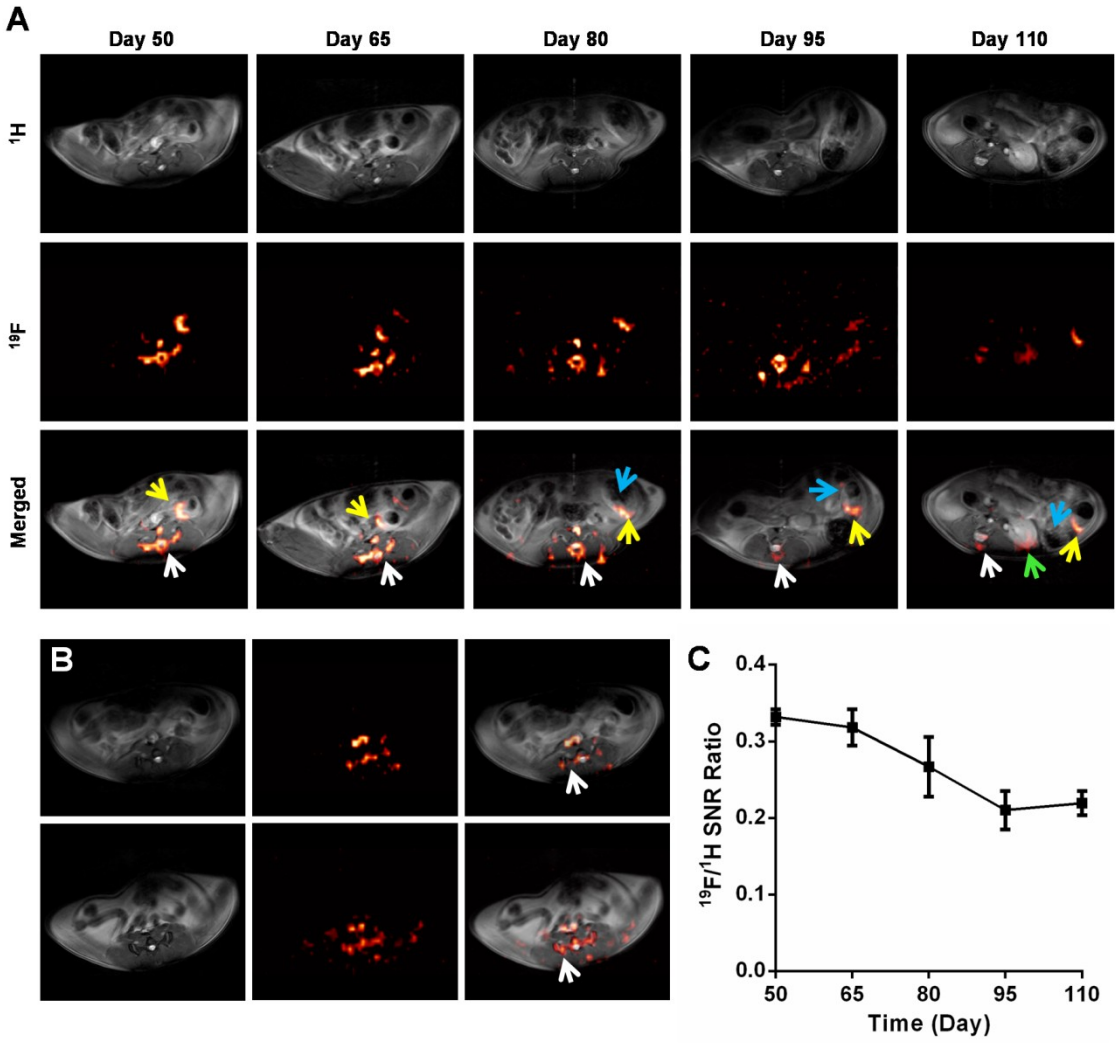

Figure 3. In vivo $^{1}H/^{19}F$ MR imaging shows PFC emulsion accumulation on colon walls and vertebra in mice. (A) Axial MR images of abdomen of CAC-induced mice from day 50, 65, 80, 95, and 110 (from left to right). Panels in top row are ^{1}H images in gray scale which show anatomical texture of mice abdomen. Middle row are ^{19}F images in hot iron color scale and the lowest row are the ^{1}H-^{19}F merged images, showing that the ^{19}F signals are coming from colon wall and vertebra (yellow and white arrows respectively). From day 80, proliferative lesions started to be detected along the ^{19}F signals on colon wall (blue arrows). ^{19}F signals were also detected from kidney at day 110 (green arrow). (B)

Axial MR images of control mice does not show ^{19}F signals from colon wall but only from vertebra (white arrow). (C) Normalized ^{19}F signal-to-noise ratio (SNR) shows that ^{19}F signal intensity decreased over time.

3.2 Co-localization of ^{19}F Signal with Inflammatory and Dysplastic Lesions Through Ex Vivo MRI

After the last *in vivo* MRI, mice were euthanized and colon tissues were excised and fixed in 4% paraformaldehyde. *Ex vivo* MR imaging was done to confirm the results from *in vivo* MRI and exactly co-localize the inflammatory sites and dysplastic lesions with ^{19}F signals. Similar to *in vivo* images, ^{19}F signals were concentrated on the colon wall showing several distinct foci (Fig. 4A). Once the colon tissues were cut and opened longitudinally, most of descending colon segments with ^{19}F signals contained adenomas or dysplastic lesions while all the colon segments without ^{19}F signals did not have any kinds of proliferative lesions (Fig. 4B). H&E stained sections from paraffin-embedded tissues were compared with corresponding axial MR images. The strong ^{19}F signals turned out to be coming from either regions with severe inflammation characterized by rich phagocytic immune cell infiltration or dysplastic lesions (Fig. 4C).

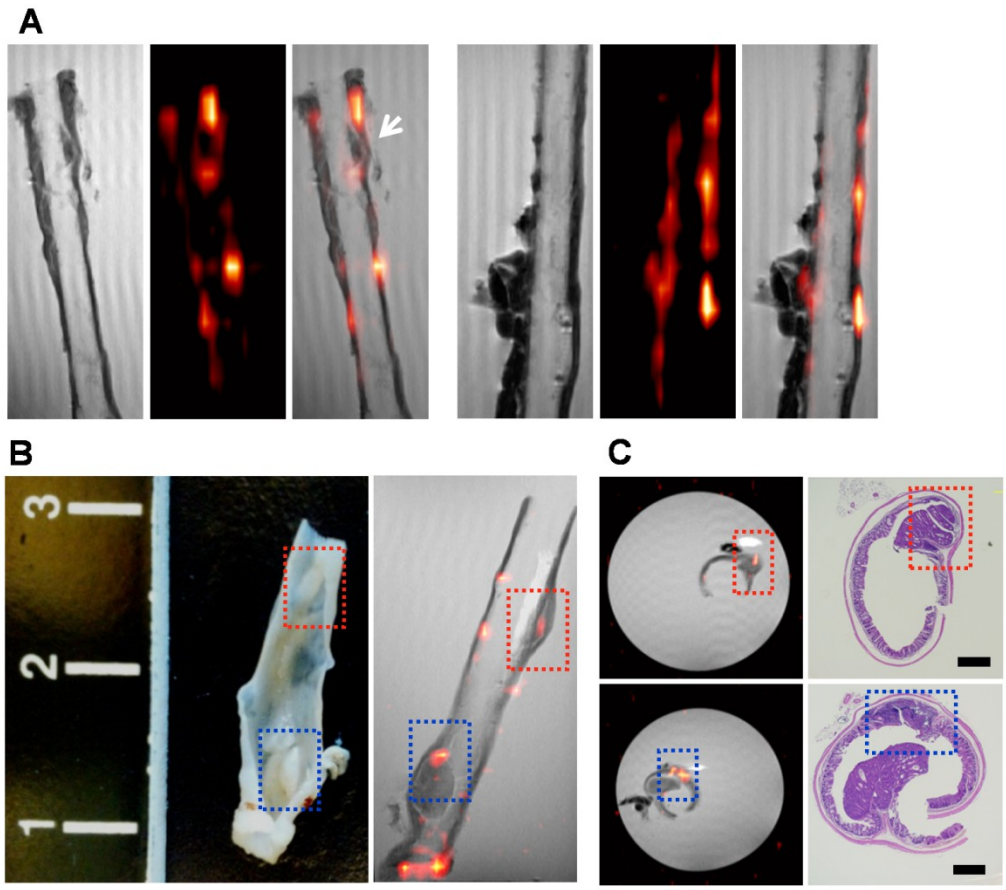

Figure 4. *Ex vivo* MR images show co-localization of ^{19}F signals with adenoma and inflammatory sites. (A) Representative sagittal MR images of excised colon fixed in 4% paraformaldehyde. ^{1}H images (gray scale) were merged with corresponding ^{19}F images (hot iron scale) to identify the origination of ^{19}F signals. White arrow indicates an adenoma grown from a ^{19}F-positive inflammatory site. (B) Excised colons were grossly observed for comparison with corresponding MR images. Boxes of same color coding (red and blue) indicate the adenoma in thegross image of a colon segment and MR image. Both of these adenomas show ^{19}F signals from MR image (scale unit: cm). (C) Axial *ex vivo* MR images were compared with corresponding regions on H&E stained sections. Co-localization of ^{19}F signals with either an adenoma (red box) or an inflammatory site

(blue box) was observed (scale bar: 500 μm).

3.3 ^{19}F Signal Intensity Has High Correlation with Histological Scores of Inflammation and Dysplasia

To confirm whether ^{19}F signal indicates higher severity of inflammation and risk of CAC development, histological sections of colon tissues were analyzed (Fig. 5A). Multiple colon segments from each CAC-induced mouse were made and classified to either segments with ^{19}F signal or those without ^{19}F signal. Inflammation in H&E stained sections were analyzed through six parameters, which are 1) area involved, 2) edema, 3) crypt loss, 4) erosion, 5) polymorphonuclear cell (PMNC) infiltration, and 6) mononuclear cell (MNC) infiltration into lamina propria. Dysplastic lesions were also scored based on their sizes and invasiveness.

In most of the parameters, sections from colon segments with ^{19}F signal had higher scores than those without the signals, with especially significant difference observed in MNC infiltration criteria (Fig. 5B). Dysplasia scores and total colitis score, the sum of scores from all criteria, were also compared between two groups, and segments with ^{19}F signal had significantly higher scores in both cases (Fig. 5C). Comparison between the segments from ascending colon and from descending colon showed that the latter group had higher score (Fig. 6A).

For the segments with ^{19}F signal, the normalized ^{19}F SNRs were correlated with histological scores of colitis and dysplasia. Segments from both ascending colon and descending colon showed a significant correlation with the total colitis score (Fig 6B,C). To confirm that severe inflammation has high risk of developing dysplasia, descending colon segments were further classified into either those with dysplasia or without

dysplasia. Dysplasia groups had significantly higher total colitis score and normalized ^{19}F SNR (Fig. 6D, E).

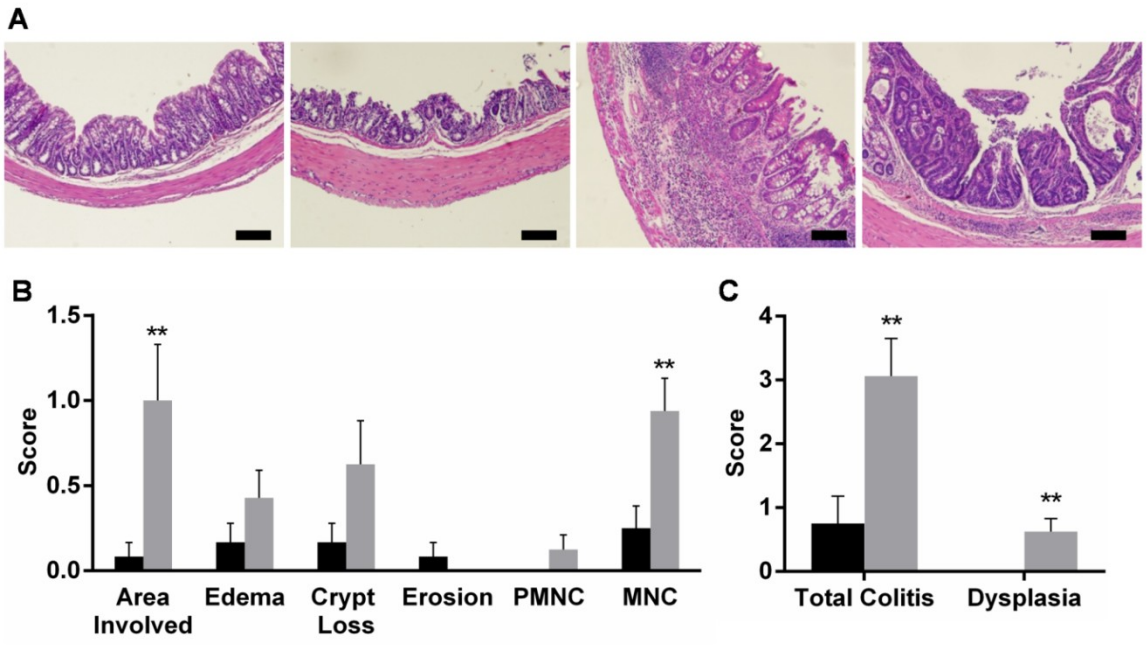

Figure 5. Representative H&E (hematoxylin& eosin)-stained sections from colons and inflammation scores of colon segments. (A) H&E stained sections of colon segments from 1) control mouse, 2) CAC-induced mouse but without ^{19}F signal, 3) CAC-induced mouse with ^{19}F signal, and 4) adenoma with ^{19}F signal (from left to right). Sections of segments with ^{19}F signal shows much more inflammation than those without ^{19}F signal, characterized by significant leukocyte infiltration and thick colon wall (scale bar = 200μm). (B) Colon segments with ^{19}F signal (gray) has higher histological scores than segments without the signal (black) from most of the parameters. Significant differences were observed in area involved ($p = 0.008$) and mononuclear cell (MNC) infiltration ($p = 0.007$) criteria. (C) Total colitis score was calculated by sum of the scores from all of criteria. Colon segments with ^{19}F signals have significantly higher total colitis score ($p = 0.003$) and dysplasia score ($p = 0.004$) than those without the signal. One-tailed t-test was performed for statistical analysis with the significance level of 0.05.

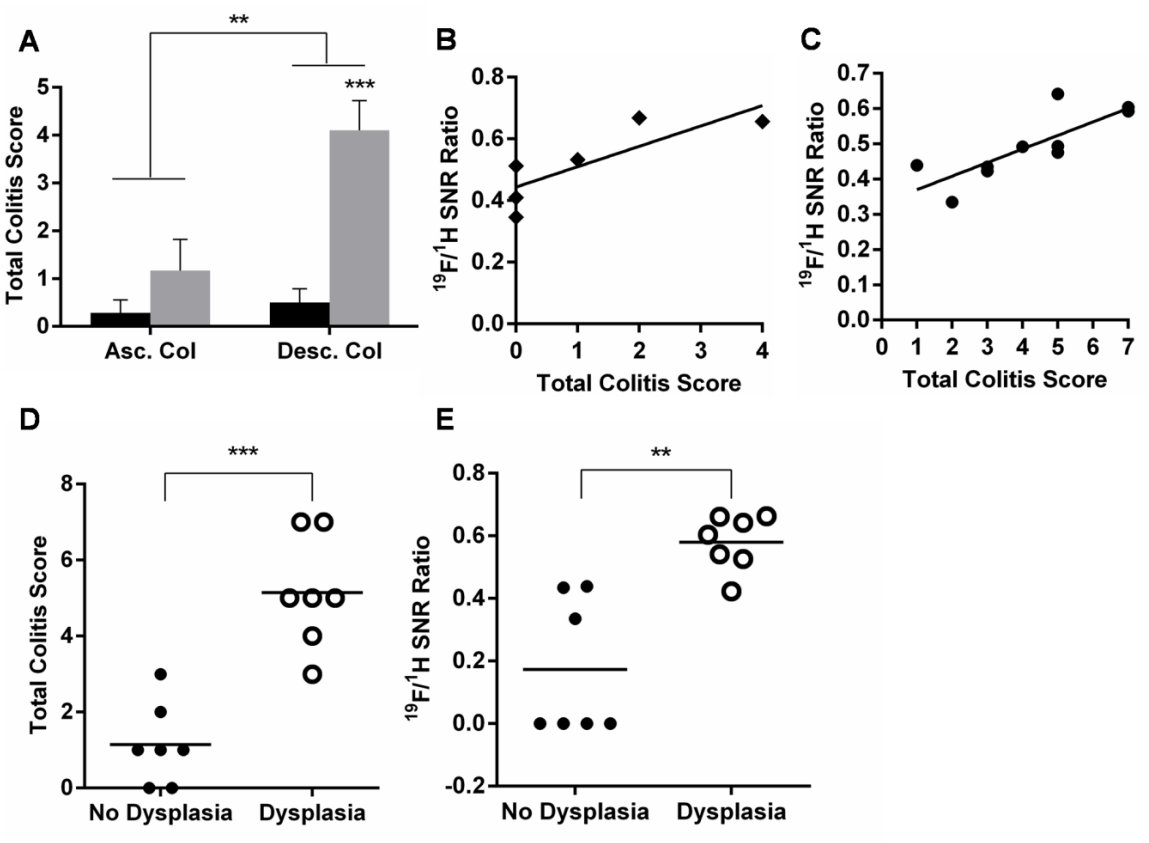

Figure 6. Correlation between normalized ^{19}F SNR and histological disease scores. (A) Comparison of total colitis score between ascending colon and descending colon. Descending colon shows much higher score than ascending colon ($p = 0.006$). Within the descending colon, segments with ^{19}F signal (gray) has significantly higher score than those without the signal (black) ($p = 0.0002$). (B) Correlation between normalized ^{19}F SNR and total colitis score of ascending colon segments ($R^2 = 0.673$). (C) Correlation between normalized ^{19}F SNR with the total colitis score in descending colon segments ($R^2 = 0.652$). (D) Total colitis scores of descending colon segments either with dysplasia or without dysplasia ($p = 0.0004$). (E) Normalized ^{19}F SNRs of descending colon segments either with dysplasia or without dysplasia ($p = 0.002$). One-tailed t-test was performed for statistical analysis with the significance level of 0.05.

4. Discussion

In this study, for the first time, ^{19}F MRI was used to image the transition of inflammatory sites into dysplastic lesions, and the clinical potential of ^{19}F MRI for earlier non-invasive CAC diagnosis has been demonstrated. The *in vivo* MR images showed ^{19}F signals on colon wall with patchy distribution, representing accumulation of macrophages on inflammatory sites. The *in vivo* data were validated by *ex vivo* images and H&E stained sections, which showed exact co-localization with dysplastic lesions and ^{19}F-positive inflammatory sites. Histological scores of inflammation and dysplasia showed significant correlation with the intensity of ^{19}F signals, indicating that the severity of inflammation can be non-invasively measured.

The accumulation of *in situ*labeled macrophages in inflammatory sites was represented by a patchy distribution of ^{19}F signals on colon wall. These ^{19}F signal patches enabled exact localization of inflammatory sties and measuring their severity, suggesting the possible utility of ^{19}F MRI for making therapeutic decisions and more selective treatment of colitis and CAC through intraoperative image guidance. Since PFC emulsions label most of the circulating leukocytes and tissue macrophages, other sites in mouse body such as spleen, liver, and vertebra (bone marrow) that naturally contain high number of macrophages also showed high ^{19}F signals (67, 68). Although ^{19}F MRI requires longer time of acquisition (TA) than ^{1}H MRI due to the lower sensitivity, the total TA of ^{1}H and ^{19}F imaging per mouse in this study was around 15 minutes, which is reasonable in both preclinical and clinical studies.

For accurate measurement of ^{19}F signal intensity, ^{19}F SNR was normalized to the SNR of corresponding^{1}H image. All the factors involved in MRI that are out of operators'

control such as coil sensitivity, field homogenization and receiver gain can be corrected through the normalization, and comparison of ^{19}F signal intensities among animals and various days can be made. The normalized ^{19}F SNR from *in vivo* imaging showed that there was a steady decrease in ^{19}F signal over time, while tumor development started to be observed from day 80 (Fig. 3B). This decrease in ^{19}F signal intensity may indicate the recovery from inflammation due to the termination of DSS administration, but further studies are needed to fully illuminate the reason and implication of decrease in ^{19}F signal intensity over time.

The correlation of normalized ^{19}F SNR to histological disease scores showed that ^{19}F signals accurately represent the severity of inflammation and dysplasia development. The segment with ^{19}F signals had higher scores from most of the criteria used for inflammation assessment than those without the signals. The most significant difference was observed in MNC infiltration criteria, while PMNC infiltration criteria did not show a significant difference. This phenomenon also supports the selective *in situ* PFC emulsion labeling of macrophages. Total colitis score, which is sum of the scores from all criteria, was also well represented by normalized ^{19}F SNR. Total colitis scores of segments from a descending colon were significantly higher than those from an ascending colon (Fig. 6A). Previous studies have shown that descending colon is much more damaged than ascending colon upon DSS treatment and more susceptible to tumor growth (65). All the adenomas and dysplastic lesions appeared in this study were also from the descending colon.

Further analysis of the colon segments with ^{19}F signal showed that ^{19}F signals in the segments from both ascending and descending colon have high correlation with the

total colitis score, indicating normalized ^{19}F SNR well represents the severity of inflammation. Descending colon segments were further analyzed by comparing the segments with dysplasia and without dysplasia. The former group showed significantly higher total colitis score and normalized ^{19}F SNR, showing the potential of finding dysplastic lesions depending on the intensity of ^{19}F signals. Thus, ^{19}F signals indicate not just the severity of inflammation but also the progress to dysplastic lesions.

Early diagnosis leads to the most effective treatment of cancer. As CAC is known to have lower survival rate than sporadic colorectal cancer, earlier diagnosis is even more crucial (69). Currently, colonoscopy and mucosal biopsy are widely used for diagnosis of bowel diseases and detection of tumor development. However, this method is invasive and time-consuming, which makes patients hesitate for frequent monitoring. PET/CT has been studied for non-invasive imaging of inflammation and tumor development, but it involves radiation and spatial resolution is low. Since ^{19}F MRI is non-invasive and depends on macrophage infiltration rather than the macroscopic appearance of lesions, it overcomes the limitations of previous imaging methods and enables earlier diagnosis.

Overall, IBD significantly increases the risk of developing CAC. ^{19}F MRI has a potential of predicting CAC development by tracking inflammatory sites and dysplastic lesions in the colon. Considering the functional relationship between inflammation and cancer, it is expected that ^{19}F MRI can also be used in earlier diagnosis of many types of cancer in future.

5. Future Studies

Although tracking macrophage burden can be used to measure the severity of inflammation, PFC emulsions can remain at the site even after macrophages leave or die and generate false signal. Thus, another marker for inflammation and tumor development should be assessed. Perfluoro-15-crown-5-ether emulsion used in this study enables measuring pO_2 of the labeled cells and tissues by its T1 relaxation rate change depending on oxygen concentration (70, 71). Since hypoxia is accompanied by inflammation and tumor progression (72 - 74), measuring pO_2 and following its dynamics over time through ^{19}F MR will provide additional information on diagnosis of CAC development.

Intracellular labeling with nanoparticles does not affect cellular functions in most cases. However, one study showed that SPIO nanoparticle labeling of macrophages affect the cytokine production, changing the phenotype of macrophages to be anti-inflammatory (75). For mesenchymal stem cells, the differentiation lineage was affected by inhibition of chondrogenesis (76). Considering that PFC is used for anti-inflammatory agent for pulmonary diseases (77), there is a possibility that PFC emulsion labeling of macrophages can also perturb their original function.

One of the interesting observations from this study is that the ^{19}F signals from *in vivo* images kept decreasing over time. Since dysplastic lesions have been developing during this period, the decrease of ^{19}F signal itself may represent the transition from inflammation to dysplastic lesions. To further investigate, cohort of mice can be sacrificed at several time points and the colons can be histologically analyzed to observe the disease state and correlated with ^{19}F signals.

PFC emulsions can be used not just for diagnostics but also for therapeutics by

incorporating lipophilic drugs in lipid surfactants or conjugating the surface with targeting moieties or ligands (78). Recently, celecoxib, a cyclooxygenase-2 (COX-2) specific inhibitor, has been incorporated into PFC nanoemulsion to change the phenotype of macrophages from tumor-promoting to tumor-suppressing (79). This new theranostic method can be used to mitigate the severe inflammatory response and prevent tumor progression.

In summary, ^{19}F MRI of PFC emulsions have a high potential of being used for thorough evaluation and therapy of tumor progression from inflammatory sites. Degree of hypoxia, which is also a marker of inflammation and tumor development, can be measured along with ^{19}F signal intensity, and PFC emulsions can be rendered as a theranostic agent. All these measurements and observations can be done non-invasively, overcoming the inconvenience of current IBD and CAC diagnosis based on endoscopy and biopsy. Further studies will polish the new ^{19}F MRI method described here and enable clinical application to enhance the diagnosis and treatment of inflammation-driven tumors.

References

[1] Coussens LM, Werb Z. Inflammation and cancer. *Nature*. 2002;420:860-867

[2] Mantovani A, Allavena P, Sica A, Balkwill F. Cancer-related inflammation. *Nature*. 2008;454:436-444

[3] Balkwill F, Charles KA, Mantovani A. Smoldering and polarized inflammation in the initiation and promotion of malignant disease. *Cancer Cell*. 2005;7:211-217

[4] Karin M. Nuclear factor-κB in cancer development and progression. *Nature*. 2006;441:431-436.

[5] Yu H, Kortylewski M, Pardoll D. Crosstalk between cancer and immune cells: role of STAT3 in the tumor microenvironment. *Nat Rev Immunol*. 2007;7:41-51

[6] Balkwill F, Mantovani A. Inflammation and cancer: back to Virchow? *Lancet*. 2001;357:539-545.

[7] Flossman E, Rothwell PM. Effect of aspirin on long-term risk of colorectal cancer: consistent evidence from randomised and observational studies. *Lancet*. 2007;369:1603-1613

[8] Tenesa A, Dunlop MG. New insights into the aetiology of colorectal cancer from genome-wide association studies. *Nat Rev Genet*. 2009;10:353-358

[9] Grivennikov SI. Inflammation and colorectal cancer: colitis-associated neoplasia. *SeminImmunopathol*. 2013;35:229-244

[10] Rubin DC, Shaker A, Levin MS. Chronic intestinal inflammation: inflammatory bowel disease and colitis-associated colon cancer. *Front Immunol*. 2012;3:107

[11] Terzic J, Grivennikov S, Karin E, Karin M. Inflammation and colon cancer. *Gastroenterology*. 2010;138(6):2101-2114.

[12] Itzkowitz SH, Yio X. Inflammation and cancer IV. Colorectal cancer in inflammatory bowel disease: the role of inflammation. *Am J PhysiolGastrotintest Liver Physiol*. 2004;287:G7-G17

[13] Ullman TA, Itzkowitz SH. Intestinal inflammation and cancer. *Gastroenterology*. 2011;140:1807-1816

[14] Rutter M, Saunders B, Wilkinson K et al. Severity of inflammation is a risk factor for colorectal neoplasia in ulcerative colitis. *Gastroenterology*. 2004;126:451-459

[15] Eaden JA, Abrams KR, Mayberry JF. The risk of colorectal cancer in ulcerative colitis: a meta-analysis. *Gut*. 2001;48:526-535

[16] Westbrook AM, Szakmary A, Schiestl RH. Mechanisms of intestinal inflammation and development of associated cancers: lessons learned from mouse models. *Mutat Res*. 2010;705:40-59

[17] Canavan C, Abrams KR, Mayberry JF. Meta-analysis: colorectal and small bowel cancer risk in patients with Crohn's disease. *Aliment Pharmacol Ther*. 2006;23:1097-1104

[18] Farraye FA, Odze RD, Eaden J, Itzkowitz SH. AGA technical review on the diagnosis and management of colorectal neoplasia in inflammatory bowel disease. *Gastroenterology*. 2010;138:746-774

[19] Kuster W, Pascoe L, Purrmann J, Funk S, Majewski F. The genetics of Crohn disease: complex segregation analysis of a family study with 265 patients with Crohn disease and 5387 relatives. *Am J Med Genet*. 1989;32:105-108

[20] Hommes DW, van Deventer JH. Endoscopy in inflammatory bowel diseases. *Gastroenterology*. 2004;126:1561-1573

[21] Fefferman DS, Farrell RJ. Endoscopy in inflammatory bowel disease: indications, surveillance, and use in clinical practice. *Clin Gastroenterol Hepatol*. 2005;3:11-24

[22] Neumann H, Vieth M, Langner C, Neurath MF, Mudter J. Cancer risk in IBD: How to diagnose d how to manage DALM and ALM. *World J Gastroenterol*. 2011;17(27):3184-3191

[23] Nagasako K, Iizuka B, Ishii F, Miyazaki J, Fujimori T. Colonoscopic diagnosis of dysplasia and early cancer in long-standing colitis. *J Gastroenterol*. 1995;30:36-39

[24] Riddell RH, Goldman H, Ransohoff DF et al. Dysplasia in inflammatory bowel disease: standaradized classification with provisional clinical applications. *Hum Pathol*. 1983;14:931-968

[25] Viani KL, Doyle LA, Farraye FA, Odze RD. Polypoid lesions in inflammatory bowel disease. *Tech Gastrointest Endosc*. 2013;15:113-120

[26] Bernstein CN, Shanahan F, Weinstein WM. Are we telling patients the truth about surveillance colonoscopy in ulcerative colitis? *Lancet*. 1994;343:71-74

[27] Itzkowitz SH, Present DH. Consensus conference: Colorectal cancer screening and surveillance in inflammatory bowel disease. *Inflamm Bowel Dis*. 2005;11:314-321

[28] Kiesslich R, Fritsch J, Holtmann M et al. Methylene blue-aided chromoendoscopy for the detection of intraepithelial neoplasia and colon cancer in ulcerative colitis. *Gastroenterology*. 2003;24:880-888

[29] Machida H, Sano Y, Hamamoto Y et al. Narrow-band imaging in the diagnosis of colorectal mucosal lesions: a pilot study. *Endoscopy*. 2004;36:1-5

[30] Neumann H, Kiesslich R, Wallace MB, Neurath MF. Confocal laser endomicroscopy: technical advances and clinical applications. *Gastroenterology*. 2010;139:388-392

[31] Jackson JR, Seed MP, Kircher CH, WIlloughby DA, Winkler JD. The codependence of angiogenesis and chronic inflammation. *FASEB J*. 1997;11(6):457-465

[32] Balfour SR. Pathogenesis and immune mechanisms of chronic inflammatory bowel diseases. *Am J Gastroenterol*. 1997;92:5s-11s

[33] Geboes K, Riddell R, Ost A et al. A reproducible grading scale for histological assessment of inflammation in ulcerative colitis. *Gut*. 2000;47:404-409

[34] Meisner RS, Spier BJ, Einarsson S et al. Pilot study using PET/CT as a novel, noninvasive assess,emt pf disease activity in inflammatory bowel disease. *Inflamm Bowel Dis*. 2007;13:993-1000

[35] Hawkins RA, Hoh C, Glaspy J et al. The role of positron emission tomography in oncology and other whole-body applications. *Semin Nucl Med*. 1992;22:268-284

[36] Schreyer AG, Seitz J, Feuerbach S, et al. Modern imaging using computer tomography and magnetic resonance imaging for inflammatory bowel disease (IBD). *Inflamm Bowel Dis.* 2004;10:45-54

[37] Sempere GA, Martinez Sanjuan V, Medina Chulia E, et al. MRI evaluation of inflammatory activity in Crohn's disease. *Am J Roentgenol.* 2005;184:1829-1835

[38] Janowski M, Bulte JWM, Walczak P. Personalized nanomedicine advancements for stem cell tracking. *Adv Drug Deliv Rev*. 2012;64:1488-1507

[39] Ahrens ET, Bulte JWM. Tracking immune cells *in vivo* using magnetic resonance imaging. *Nat Rev Immunol*. 2013;13:755-763

[40] Thorek DL, Chen AK, Czupryna J, Tsourkas A. Superparamagnetic iron oxide nanoparticle probes for molecular imaging. *Ann Biomed Eng*. 2006;34:23-38

[41] Kanno S, Wu YJ,Lee PC et al. Macrophage accumulation associated with rat cardiac allograft rejection detected by magnetic resonance imaging with ultrasmall syperparamgnetic iron oxide particles. *Circulation*. 2001;104:934-938

[42] Kooi ME, Cappendijk VC, Cleutjens KB et al. Accumulation of ultrasmall superparamagnetic particles of iron oxide in human atherosclerotic plaques can be detected by *in vivo* magnetic resonance imaging. *Circulation*. 2003;107:2453-2458

[43] Dousset V, Delalande C, Ballarino L et al. *In vivo* macrophage activity imaging in the central nervous system detected by magnetic resonance. *Magn Reson Med*. 1999;41:329-333

[44] Enochs WS, Harsh G, Hochberg F, Weissleder R. Improved delineation of human brain tumors on MR images using a long-circulating, superparamagnetic iron oxide agent. *J Magn Reson Imaging*. 1999;9:228-232

[45] Saleh A, Schroeter M, Jonkmanns C et al. In vivo MRI of brain inflammation in human ischaemic stroke. *Brain*. 2004;127:1670-1677

[46] Weissleder R, Nahrendorf M, Pittet MJ. Imaging macrophages with nanoparticles. *Nat Mater*. 2014;13:125-138

[47] Riess JG. Oxygen carriers ("blood substitutes") - raison d'etre, chemistry, and some physiology. *Chem Rev*. 2001;101:2797-2919.

[48] Krafft MP, Riess JG. Perfluorocarbons: life sciences and biomedical uses dedicated to the memory of Professor Guy Ourisson, a true renaissance man. *J Polym Sci, Part A: Polym Chem*. 2007;45:1185-1198

[49] Krafft MP. Fluorocarbons and fluorinated amphiphiles in drug delivery and biomedical research. *Adv Drug Deliv Rev*. 2001;47:209-228

[50] Flaim SF. Pharmacokinetics and side effects of perfluorocarbon-based blood substitutes. *Artif Cells Blood Substit Immobil Biotechnol*. 1994;22:1043-1054

[51] Lowe KC. Engineering blood: synthetic substitues from fluorinated compounds. *Tissue Eng*. 2003;9:389-399

[52] Kadayakkara DK, Ranganathan S, Young W, Ahrens ET. Assaying macrophage activity in a murine model of inflammatory bowel disease using fluorine-19 MRI. *Lab Invest*. 2012;92:636-645

[53] Ruiz-Cabello J, Barnett BP, Bottomley PA, Bulte JWM. Fluorine (^{19}F) MRS and MRI in Biomedicine. *NMR Biomed*. 2011;24:114-129

[54] Ahrens ET, Zhong J. *In vivo* MRI cell tracking using perfluorocarbon probes and fluorine-19 detection. *NMR Biomed*. 2013;

[55] Ahrens ET, Young WB, Xu H et al. Rapid quantification of inflammation in tissue samples using perfluorocarbon emulsion and fluorine-19 nuclear magnetic resonance. *Biotechniques*. 2011;50:229-234

[56] Hertlein T, Strum V, Kircher S et al. Visualization of abscess formation in a murin thigh infection model of Staphylococcus aureus by F-19-magnetic resonance imaging (MRI). *PLoS One*. 2011;6(3):18246

[57] Ebner B, Behm P, Jacoby C et al. Early assessment of pulmonary inflammation by (19)F MRI in vivo. *Circ Cardiovasc Imaging*. 2010;3:202-210

[58] Flogel U, Ding Z, Hardung H, et al. *In vivo* monitoring of inflammation after cardiac and cerebral ischemia by fluorine magnetic resonance imaging. *Circulation*.

2008;118:140-148.

[59] Gordon S, Taylor PR. Monocyte and macrophage heterogeneity. *Nat Rev Immunol*. 2005;5:953-964

[60] Rugtveit J, Brandtzaeg P, Halstensen TS, Fausa O, Scott H. Increased macrophage subset in inflammatory bowel disease: apparent recruitment from peripheral blood monocytes. *Gut*. 1994;35:669-674.

[61] Mahida YR. The key role of macrophages in the immunopathogenesis of inflammatory bowel disease. *Inflamm Bowel Dis*. 2000;6:21-33

[62] Noth U, Porrissey SP, Deichmann R et al. Perfluoro-15-crown-5-ether labeled macrophages in adoptive transfer experimental allergic encephalomyelitis. *Artif Cell Blood Sub*. 1997;25:243-254

[63] Ratner AV, Muller HH, Bradley-Sumpson B et al. Detection of tumors with 19F magnetic resonance imaging. *Invest Radio*. 1988;23:361-364

[64] Neufert C, Becker C, Neurath MF. An inducible mouse model of colon carcinogenesis for the analysis of sporadic and inflammation-driven tumor progression. *Nat Protoc*. 2007;2(8):1998-2004

[65] Thaker AI, Shaker A, Rao MS, Ciorba MA. Modeling colitis-associated cancer with azoxymethane (AOM) and dextran sulfate sodium (DSS). *J Vis Exp* 2012;67, e4100

[66] Hogan SP, Seidu L, Blanchard C et al. Resistin-like molecule b regulates innate colonic function Barrier integrity and inflammation susceptibility. *J Allergy ClinImmunol*. 2006;118(1):257-268

[67] Diaz-Lopez R, Tsapis N, Fattal E. Liquid perfluorocarbons as contrast agents for ultrasonography and ^{19}F-MRI. *Pharmaceut Res*. 2010;27:1-16

[68] Sotak CH, Hees PS, Huang H et al. A new perfluorocarbon for use in fluorine-19 magnetic resonance imaging and spectroscopy. *Magn Reson Med*. 1993;29:188-195

[69] Watanabe T, Konishi T, Kishimoto J et al. Ulcerative colitis-associated colorectal cancer shows a poorer survival than sporadic colorectal cancer: A nationwide Japanese study. *Inflamm Bowel Dis*. 2011;17(3):802-808

[70] Kadayakkara DK, Janjic JM, Pusateri LK, Young W, Ahrens ET. *In vivo* observation of intracelllularoximetry in perfluorocarbon-labeled glioma cells and chemotherapeutic response in the CNS using fluorine-19 MRI. *MagnReson Med*. 2010;64:1252-1259

[71] Mason RP, Shukla H, Antich PP. *In vivo* oxygen tension and temperature: simultaneous determination using 19F NMR spectroscopy of perfluorocarbon. *MagnReson Med*. 1993;23:296-302.

[72] Eltzschig HK, Carmeliet P. Hypoxia and Inflammation. *N Engl J Med*. 2011;364:656-665.

[73] Murdoch C, Muthana M, Lewis CE. Hypoxia regulates macrophage functions in inflammation. *J Immunol*. 2005;175:6257-6263

[74] Kunz M, Ibrahim SM. Molecular responses to hypoxia in tumor cells. *Mol Cancer.* 2003;2:23

[75] Siglienti I, Bendszus M, Kleinschnitz C, Stoll G. Cytokine profile of iron-ladene macrophages: implications for cellular magnetic resonance imaging. *J Neuroimmunol*. 2006;173:166-173

[76] Kostura L, Kraitchman DL, Mackay AM, Pittenger MF, Bulte JWM. Feridex labeling of mesenchymal stem cells inhibits chondrogenesis but not adipogenesis or osteogenesis. *NMR Biomed*. 2004;17:513-517

[77] Lehmler H. Anti-inflammatory effects of perfluorocarbon compounds. *Expert Rev Resp Med*. 2008;2:273-289

[78] Kaneda MM, Caruthers S, Lanza GM, Wicklines SA. Perfluorocarbon nanoemulsions for quantitative molecular imaging and targeted therapeutics. *Ann Biomed Eng*. 2009;37:1922-1933

[79] Patel SK, Zhang Y, Pollock JA, Janjic JM. Cyclooxygenase-2 inhibiting perfluoropoly(ethylene glycol) ether theranostic nanoemulsions--in vitro study. *PLoS One*. 2013;8:e55802

Curriculum Vitae

Soo Hyun Shin received B.S. degree in Biomedical Engineering from the Johns Hopkins University in 2012. During his Bachelor's study, he served as a research assistant in Institute for Cell Engineering at the Johns Hopkins University School of Medicine. He also worked in Department of Biomedical Engineering, College of Health Science in Korea University and Center for Biomaterials in Korea Institute of Science and Technology (KIST) as an assistant. Under the guidance of Dr. Jeff W.M. Bulte, he completed the thesis in Department of Biomedical Engineering at the Johns Hopkins University in 2014. From 2014 August to 2017 July, he is expected to work as a research scientist in Molecular Imaging and Therapy branch at National Cancer Center (NCC), Korea.